# Multitemporal Unmixing of Medium-Spatial-Resolution Satellite Images: A Case Study Using MERIS Images for Land-Cover Mapping

Raúl Zurita-Milla, Luis Gómez-Chova, *Member, IEEE*, Luis Guanter, Jan G. P. W. Clevers, and Gustavo Camps-Valls, *Senior Member, IEEE*

***Abstract*—Data from current medium-spatial-resolution imaging spectroradiometers are used for land-cover mapping and land-cover change detection at regional to global scales. However, few landscapes are homogeneous at these scales, and this creates the so-called mixed-pixel problem. In this context, this study explores the use of the linear spectral mixture model to extract subpixel land-cover composition from medium-spatial-resolution data. In particular, a time series of MEdium Resolution Imaging Spectrometer (MERIS) full-resolution (FR; pixel size of 300 m) images acquired over The Netherlands is used to illustrate this study. The Netherlands was selected because of the following: 1) the fragmentation of its landscapes and 2) the availability of a high-spatial-resolution land-cover data set (LGN5) which can be used as a reference. The question then is to what extent a multitemporal unmixing of MERIS FR data delivers land-cover information comparable with the one provided by the LGN5. To this end, fully constrained linear spectral unmixing is applied to each individual MERIS image and to the multitemporal composite. The unmixing results are validated at both subpixel and per-pixel scales and at two thematic aggregation levels (12 and 4 land-cover classes). The obtained results indicate that the described unmixing approach yields moderate results for the 12-class case and good results for the 4-class case. These results might be explained by MERIS preprocessing steps, gridding effects, vegetation phenophases, and spectral class separability.**

***Index Terms*—Heterogeneity, land cover, MEdium Resolution Imaging Spectrometer (MERIS), multitemporal unmixing, subpixel, time series.**

Manuscript received October 29, 2010; revised February 4, 2011 and March 30, 2011; accepted May 1, 2011. This work was supported in part by the Dutch SRON GO Program (EO-061) and in part by the Spanish Ministry for Education and Science under Projects AYA2008-05965-C04-03 and CONSOLIDER/CSD2007-00018.

R. Zurita-Milla is with the Faculty of Geo-information Science and Earth Observation (ITC), University of Twente, 7500 AE Enschede, The Netherlands (e-mail: zurita-milla@itc.nl).

L. Gómez-Chova and G. Camps-Valls are with the Image Processing Laboratory, University of Valencia, 46980 Valencia, Spain (e-mail: luis.gomez-chova@uv.es; gustavo.camps@uv.es).

L. Guanter is with the Atmospheric, Oceanic and Planetary Physics, Clarendon Laboratory, University of Oxford, OX1 3PU Oxford, U.K. (e-mail: luis.guanter@uv.es).

J. G. P. W. Clevers is with the Centre for Geo-Information, Wageningen University, 6700 AA Wageningen, The Netherlands (e-mail: jan.clevers@wur.nl).

Color versions of one or more of the figures in this paper are available online at http://ieeexplore.ieee.org.

Digital Object Identifier 10.1109/TGRS.2011.2158320

## I. Introduction

REMOTE sensing images are acquired using the so-called "raster data model" [1]. This model consists of nonoverlapping areal units called pixels that are arranged in a regular grid [2]. This means that remote sensing images are acquired using predefined pixel and grid sizes. Traditional image processing techniques work according to this acquisition model: The recorded signal is processed to create products where a unique value (e.g., surface reflectance or class label) is assigned to each pixel. In principle, this approach is useful when the pixel size and the spatial scale of the phenomena under study closely match. However, even in this case, the raster model will cause the so-called mixed-pixel problem. Mixed pixels are pixels that either contain information from more than one material or when they contain information from only one material this is not homogeneous in all its properties [3]–[5].

Finding a solution for the mixed-pixel problem is important for a number of remote sensing applications. First of all, it is important for land-cover mapping, as land-cover area estimation can only be accepted if the classification accuracy is very good and if the impact of mixed pixels is negligible [6]. Furthermore, from a quantitative perspective, it is essential for an accurate retrieval and interpretation of biophysical and biochemical parameters [7]. Thus, it has been shown that, when there is a lot of land-cover mixing, retrieval uncertainties can be quite high [8]. In addition to this, subpixel snow cover reduces the accuracy of leaf area index and of the fraction of absorbed photosynthetically active radiation estimates [9]. The same applies to subpixel water bodies [10] and subpixel cloud coverage [11].

This paper deals with the first application: land-cover mapping, particularly with regional land-cover mapping using the MEdium Resolution Imaging Spectrometer (MERIS) [12]. MERIS was selected because it provides data with a spectrally enhanced configuration (15 narrow bands in the visible and near-infrared) and with a quasi-daily global coverage (revisit time of two to three days). These two characteristics might help to overcome the fact that MERIS images usually contain many mixed pixels as this sensor operates with a nominal pixel size of 300 m.

The first characteristic, 15 narrow bands, facilitates the use of the most established technique to deal with mixed pixels, the

linear mixing model, since the number of land-cover classes that can be unmixed is, in principle, limited by the number of bands (cf. Section III-A for more details). The second characteristic, two-to-three-day revisit time, allows the use of temporal patterns (e.g., vegetation phenology) to discriminate among land-cover types.

At this point, it is worth noting that several unmixing approaches can be found in literature (see [13] and [14] for an extensive review). These approaches are typically categorized into linear or nonlinear. Nonlinear unmixing is usually considered when working with intimate mixtures (e.g., complex mineralogical composition [15]) or when working with land-cover types with a clear 3-D structure (e.g., orchard fields [16]). In this paper, nonlinear effects are not deemed important because of the medium spatial resolution. At this spatial scale, multiple photon scattering and lateral radiation fluxes are not very critical, as illustrated by other studies where data from the MODerate-resolution Imaging Spectrometer (MODIS) were unmixed using a linear model [17], [18]; these references are also examples of multitemporal unmixing. However, MODIS only has two bands (red and near-infrared) at a comparable spatial resolution of 250 m. This limits the spectral characterization of land-cover types and, as a consequence, the number and type of land-cover classes that can be unmixed. Thus, the aim of this study is to evaluate the possibilities of unmixing MERIS time series to generate land-cover information comparable[1] with the one that can be obtained from high-spatial-resolution (Landsat-like) sensors. This would facilitate a consistent monitoring of land-cover status over areas where the production of yearly land-cover maps at high spatial resolution remains challenging (because these areas are very heterogeneous and/or because they are frequently clouded).

The remainder of this paper is organized as follows. Section II describes the study area, the data sets used in this study, the main preprocessing steps, and the data used for validation. Section III presents the proposed unmixing method, the endmember selection procedure, and validation approaches. The unmixing results, their validation, and the possibilities to operationally use a MERIS FR time series of data to map land-cover composition are discussed in Section IV. Finally, Section V summarizes the main findings and highlights the advantages and limitations of the proposed land-cover mapping approach.

## II. Materials

### A. MERIS Full-Resolution Data

A time series of MERIS FR Level 1b (L1b) images (geolocated top-of-atmosphere (TOA) radiances) acquired over The Netherlands in 2003 was selected to illustrate this work. The Netherlands was selected as study area because of the heterogeneity of its landscapes, its relatively high cloud coverage, and the availability of an up-to-date high-spatial-resolution land-use database that can be used to validate the results (Sections II-B and II-C). The MERIS acquisition dates were chosen according to two criteria: 1) to maximize the number of valid cloud free pixels in each scene and 2) to get at least one image per month so that the phenological cycle is fully captured. Nevertheless, no suitable MERIS FR scenes were found for the months of January, March, June, September, and November. Therefore, an uneven time series of seven images is used (Fig. 1). This time series is considered to be sufficient for the purpose of this study.

The MERIS FR images were first projected into the Dutch national coordinate system (RD) using the geolocation information provided with the data. After that, a cloud screening algorithm [19] was applied to all the images to identify and mask out cloud-contaminated pixels. Then, the TOA radiances were transformed into surface reflectance using an atmospheric correction algorithm specifically designed for the processing of MERIS land pixels [20] and subsequently optimized to characterize the atmospheric state over continental surfaces: land targets, small inland water bodies, and the first 10 km of water from the shoreline (for which the atmospheric information derived over neighboring land pixels can be extrapolated) [21]. The use of the continental surfaces optimized algorithm is obviously motivated by the particular importance of water in the selected study area (The Netherlands).

### B. Reference Data Set

The fifth version of the Dutch land-use database, known as the LGN5, is used as a reference in this study. More precisely, this data set is used to both support the selection of the endmembers and create the validation data sets (cf. Section III-B and C).

The LGN5 is one of the standard data sets used at national level for applications in the fields of water management, spatial planning, and environmental management [22]. With this data set, a detailed series of land-use databases (LGN1-5) covering the period from 1990s to 2004 is made available for The Netherlands. This particular data set (LGN5) is based on a multitemporal classification of high-spatial-resolution satellite data (mostly Landsat imagery) acquired in 2003 and 2004 and several types of ancillary data (see [22] for more details). The LGN5 has a raster structure with a pixel size of 25 m, and it is given in the national RD grid. From a thematic point of view, the LGN5 maps 39 classes. However, mapping all these classes at medium resolution is unrealistic because some of them describe land-use rather than land-cover types (i.e., their mapping heavily relies on ancillary data instead of on the spectral properties of the surface) and because some classes are rather small. Consequently, the LGN5 was thematically aggregated into the 12 main land-cover types of The Netherlands. This aggregation is meant to offer a detailed distribution of the following classes: grassland, summer crops, winter crops, orchards, deciduous forest, coniferous forest, water, built-up (urban areas), greenhouses, bare soil (including sand dunes), heathlands, and swamps. A further aggregation of these 12 classes resulted in a map with four main classes: vegetation, bare soil, water, and built-up. Despite its simplified legend, the aggregation to four classes is of great interest because it can be used, for instance, as a proxy for fractional vegetation cover

[1]Here, "comparable" means that the information is similar if the same level of spatial detail is considered (obviously, high-spatial-resolution sensors have a smaller pixel size than medium-spatial-resolution sensors).

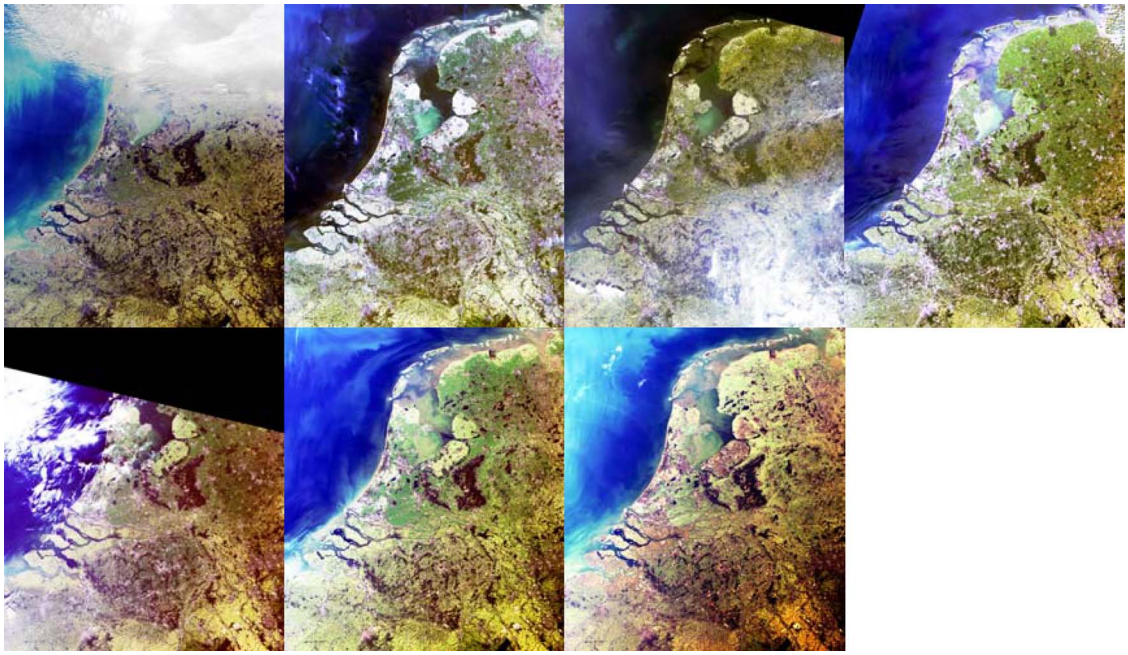

Fig. 1. Coregistered MERIS FR L1b time series acquired over The Netherlands in 2003: February 18, April 16, May 31, July 14, August 6, October 15, and December 8 (*RGB color composite of MERIS bands 6, 5, and 2—640, 550, and 460 nm, respectively*).

and because, as stated in the introduction, it might also be used to improve the retrieval of biophysical and/or biochemical parameters.

## III. Methodology

### A. Linear Spectral Unmixing

Linear spectral mixture analysis is a relatively straightforward method that is commonly used to deal with the mixed-pixel problem [13], [23], [24]. In this analysis, each pixel is modeled as a linear combination of the pure spectral response of each of the classes that are present in the pixel.

Several implementations of this method can be found in literature [14]. Here, a fully constrained linear spectral unmixing (FCLSU) was used to extract subpixel land-cover composition from the MERIS FR images because this unmixing method guarantees a physical interpretation of the results [25].

For the case of a single image acquired at date $t$, the FCLSU can be formalized as follows:

$$p_i^t = \sum_{c=1}^{nc} \left( \hat{f}_c^t \cdot \mu_{ci}^t \right) + \varepsilon_i^t \tag{1}$$

subject to

$$0 \leq \hat{f}_c^t \leq 1 \quad \sum_{c=1}^{nc} \hat{f}_c^t = 1 \tag{2}$$

where $p_i^t$ is the pixel value for band $i$ and time $t$, $\mu_{ci}^t$ is the pure signal of class $c$ in band $i$ and time $t$ (this signal is commonly known as "class endmember"), $nc$ represents the number of classes that are being unmixed (number of endmembers), and $\hat{f}_c^t$ is the estimated fraction of class $c$ present in the pixel. Finally, the term $\varepsilon_i^t$ represents the *per* band residual error. Thus, the FCLSU solves the constrained linear least-squares problem

$$\arg\min_{\hat{f}_c^t} \left\{ \sum_{i=1}^{ni} \left( p_i^t - \sum_{c=1}^{nc} \left( \hat{f}_c^t \mu_{ci}^t \right) \right)^2 \right\}. \tag{3}$$

The FCLSU was applied to each MERIS FR image (monotemporal case) as well as to a multitemporal composite of all the MERIS FR images (multitemporal case). The latter approach was implemented because several studies (e.g., [17]) have shown that linear mixture analysis can benefit from a high temporal resolution because, in this case, the classes are defined not only by their spectral signature but also by their evolution over time. Thus, the use of "temporal signatures" provides additional information to the (monotemporal) spectral signature, particularly for classes that exhibit a clear annual pattern.

In this paper, the multitemporal unmixing is implemented using a spectral-stacked approach: Pixel entities and endmembers are defined as spectral signatures of length $ni \times nt$ (where $ni$ equals the number of spectral bands and $nt$ is the number of images in the time series). Thus, the multitemporal unmixing is formulated as follows:

$$p_i^t = \sum_{c=1}^{nc} \left( \hat{f}_c^T \cdot \mu_{ci}^t \right) + \varepsilon_i^t \tag{4}$$

subject to

$$0 \leq \hat{\boldsymbol{f}}_c^T \leq 1 \quad \sum_{c=1}^{nc} \hat{\boldsymbol{f}}_c^T = 1. \tag{5}$$

However, here, $\hat{f}_c^T$ represents the estimated fraction of class $c$ that minimizes the residual error for all the dates $t$ in the time series at the same time

$$\underset{\hat{f}_c^T}{\arg\min} \left\{ \sum_{t=1}^{nt} \sum_{i=1}^{ni} \left( p_i^t - \sum_{c=1}^{nc} \left( \hat{f}_c^T \mu_{ci}^t \right) \right)^2 \right\}. \quad (6)$$

After the formulation of the multitemporal FCLSU model, it is worthy to note the following remarks. First, the relevance of each date could easily be weighted depending on the application, although in this particular work, we decided that the contribution of all dates would have an equal weight. Second, the number of dates used in the multitemporal unmixing might be pixel dependent. Among other factors, the extent of the scenes and their cloud coverage determine the number of valid pixels for each date. In this paper, each pixel is unmixed with the maximum number of valid dates. This means that the quality of the unmixing might also be pixel dependent and that, if critical (phenological) dates are missing for a number of pixels (areas), the accuracy of the results for those pixels (areas) might be lower. Finally, the multitemporal unmixing assumes that the spatial distribution of land-cover composition is fixed for the period covered by the time series [17], [18]. In this paper, this is an implicit working assumption since the LGN5 is used as a reference and this data set was produced using the same principle: Land cover is "static" for the production period.

One should also notice that the MERIS sensor is onboard the ENVISAT platform, which repeats the same orbit every 35 days [12]. This means that potentially each of the MERIS FR images selected for the analysis have been acquired from a slightly different orbit. This, in turn, implies that each image might have a slightly different observation geometry and that, therefore, some (subpixel) differences in the instantaneous field of view of each "pixel" are to be expected [26]. These orbital differences effectively imply that spatially "collocated" pixels might present a poor temporal pixel overlap, thus having a slightly different land-cover composition in time. This explains the use of the superscript "$t$" in the formulation of the monotemporal linear mixing model.

### B. Selection of Endmembers

A fundamental task in any (linear) unmixing method is the identification of the endmembers because they largely determine the quality of the unmixing. In [27], a comparative analysis of endmember selection methods using high-spatial-resolution hyperspectral data was carried out, and it was found that the best endmember selection methods are those that consider both spatial and spectral information. In this paper, we tried to follow this principle but we adjusted it to the characteristics of the data sets at hand, since the endmember selection algorithm is not the focus of this work. Thus, the endmembers were selected using a semiautomatic approach based on two conditions: 1) Endmembers must be located in spatiotemporal homogeneous areas, and 2) they must be cloud free (spectral information). Thus defined, this endmember selection method only needs a criterion of homogeneity and the MERIS cloud masks that were obtained during the preprocessing of each image.

With respect to the homogeneity criterion, we decided, for the sake of simplicity, to use a multitemporal version of the standard purity index (SPI) [28]. This index is computed using the fractional land-cover composition of each MERIS pixel for each date, which, in our case, is known, owing to the availability of a high-spatial-resolution land-cover reference data set. If such a data set is not available, expert knowledge or automatic endmember selection methods such as the ones described in [27] could be tested. Their use would, however, be challenging given that we aim at unmixing land-cover classes (i.e., not pure materials) and that we work with MERIS data (13 bands after atmospheric correction and a nominal pixel size of 300 m).

The multitemporal SPI was computed as follows:

$$SPI = \sqrt{\sum_{c=1}^{nc} \left( f_c^{\Sigma} - f_{\max}^{\Sigma} \right)^2 \Big/ (nc-1)} \quad (7)$$

with

$$f_c^{\Sigma} = \sum_{t=1}^{nt} f_c^t \quad \text{and} \quad \boldsymbol{f}_{\max}^{\Sigma} = \max\left\{ \boldsymbol{f}_1^{\Sigma}, \boldsymbol{f}_2^{\Sigma}, \ldots, \boldsymbol{f}_{nc}^{\Sigma} \right\} \quad (8)$$

where $f_c^t$ represents the fraction of class $c$ in a given MERIS pixel and for a given time $t$. In other words, $f_c^t$ is the "ground truth" computed for each MERIS image from the LGN5 12-class data set (see Section III-C for more details on how the fractions for each MERIS pixel at each date are computed) and $nt$ and $nc$ are the number of dates and the number of classes. Based on its definition, the multitemporal SPI equals one when the pixel has only one class for all the dates under study and it equals zero when the multitemporal sum of all the fractions for each land cover class $c$ is the same. Therefore, for a given pixel, the SPI ranges between 0 and 1.

"Pure" pixels were identified for each MERIS acquisition date by first applying the corresponding cloud mask to the multitemporal SPI image and then applying an SPI threshold to the remaining (cloud-free) pixels. This threshold was adaptively tuned until at least 20 pixels were found for all the 12 land-cover classes. After that, a neighborhood constraint was applied to these SPI "pure" pixels: Only the "pure" pixels surrounded by "pure" pixels of the same land-cover class were selected to compute the spectral signatures of the endmembers. In practical terms, this was implemented as an erosion filter of 3-by-3 pixels. If the total number of "pure" pixels for a given class was less than five, then the erosion filter was not applied and all the "pure" pixels identified in the previous step were selected to compute the endmember of that class. Finally, the endmembers were created by averaging the "pure" pixels identified for each land-cover class [29].

### C. Validation Data Sets

The gridding effects discussed at the end of Section III-A were considered when producing the validation data sets. For this, each MERIS pixel footprint was projected into the original LGN5 25-m grid so that the "actual land-cover fractions" seen

by MERIS at each acquisition time $t$ could be computed, i.e., $f_c^t$. After this, the subpixel land-cover fractions were assigned to the corresponding 300-by-300-m MERIS pixel. The class having the highest fractional coverage was used to produce a hard land-cover classification for each MERIS acquisition date, namely, $\omega^t = \arg\max_c\{f_c^t\}$. This processing step allows both a subpixel and a per-pixel validation of the unmixing results for each of the MERIS FR images.

In order to create a validation data set for the multitemporal unmixing, the LGN5 was spatially aggregated to match the nominal MERIS FR pixel size. To do this, a majority filter with a kernel of 12-by-12 pixels of 25 m was used to obtain a land-cover classification map at 300 m, i.e., $\omega^T$. Similar to the monotemporal case, the fractions $f_c^T$ of the different land-cover types present in each 300-by-300-m pixel were recorded.

### D. Accuracy Assessment

As stated in the previous section, the fractional maps computed from the LGN5 (25 m and 12 classes) for the particular geometry of each MERIS acquisition $f_c^t$ were used as ground truth for the validation of the corresponding monotemporal unmixings and the fractions computed while aggregating the LGN5 to 300 m $f_c^T$ were used for the validation of the multitemporal unmixing. Assuming that the unmixed fractions are correctly positioned within each pixel, a kind of overall subpixel accuracy (OSA) can be computed as follows:

$$OSA = \sum_{c=1}^{nc} d_c \Big/ \sum_{c=1}^{nc} \hat{f}_c = \sum_{c=1}^{nc} d_c$$
$$d_c = \min\{f_c, \hat{f}_c\} \tag{9}$$

where $d_c$ are the percentages of correctly classified abundance for each class. These abundances are computed as the minimum of $f_c$ and $\hat{f}_c$, which are the LGN5-based and unmixed abundances, respectively. Notice that the sum of $\hat{f}_c$ for all classes adds to unity [(2) and (5)] and, thus, has been obviated from the second equality in (9). The OSA can be computed for the monotemporal or the multitemporal case using $f_c^t$ or $f_c^T$, respectively.

After the subpixel accuracy assessment, the unmixed fractions were used to produce land-cover classification maps for each date. The class having the maximum fractional coverage was used to label each pixel, $\hat{\omega}^t = \arg\max_c\{\hat{f}_c^t\}$. Subsequently, a classical classification accuracy assessment was done by comparing these images with the land-cover maps that were computed for each date. Similarly, the hard classified multitemporal image $\hat{\omega}^T$ was validated using the 300-m aggregated LGN5 $\omega^T$ as a reference. The confusion matrix and the estimated Cohen's Kappa coefficient were used for the per-pixel accuracy assessment.

## IV. Results and Discussion

### A. MERIS Preprocessing

A visual inspection of the projected MERIS images (Fig. 1) did not show any major geometrical shift between them (besides the expected differences due to different acquisition orbit). Images also overlapped quite well the reference data set. This can be considered as a preliminary quality proof of the georeferencing information provided with the images. Although a quantitative assessment of the geolocation accuracy might have been more appropriate, here, we decided to keep it simple in order to also test the operational use of the unmixing of MERIS FR time series. Therefore, in this study, the preprocessing steps were reduced as much as possible.

With respect to the cloud-screening method, all the clouds and cloud borders were masked out. The validation of the cloud mask revealed that a small amount of pixels belonging to the classes greenhouses (sun glint on glass roofs) and bare soil (sand dunes) was identified as clouds because these classes have similar reflectance behavior as clouds. However, the classes that were misclassified represent less than 0.5% of The Netherlands, and therefore, they are not statistically representative.

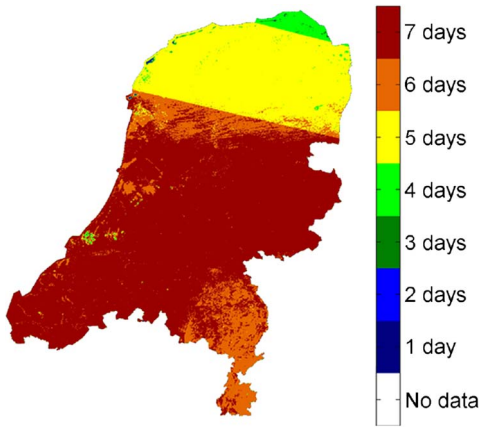


Fig. 2. Total number of usable dates.

Fig. 2 shows the number of usable dates for each MERIS FR pixel. It should be noted that the northern and southeastern parts of The Netherlands have less usable pixels than the rest of the country. This is not only because of the cloud coverage but also because some of the MERIS FR images did not cover The Netherlands completely (Fig. 1).

### B. Endmembers

Fig. 3 shows the multitemporal SPI values when considering 12 land-cover types. It is worthy to note the high heterogeneity of the landscapes, which is particularly visible on the eastern part of the country. Most of the endmembers were computed as the average of the pixels selected using an SPI threshold value of 0.95. Nevertheless, for some small classes, the SPI threshold was reduced in order to get more than 20 pixels for those classes. For instance, the SPI threshold had to be reduced to 0.87 to extract 20 "pure pixels" of the greenhouses class on cloudy dates (May 31 and August 6). For the small and sparse classes, the neighborhood constraint was, in general, not applied because very few clusters of 3-by-3 pure pixels could be found.

Fig. 4 shows the spectral signature of the endmembers selected in this study. Grassland presents the highest NIR reflectance all year round. During the months of May, July,

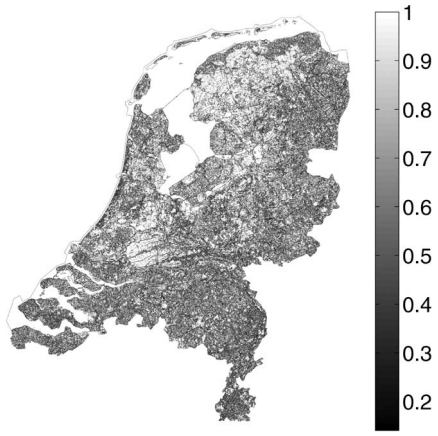


Fig. 3. Multitemporal SPI.

and August, the endmember of deciduous forest also shows high reflectance (high greening of vegetation). The rest of the vegetated classes appear to have a very similar spectral signature. Therefore, severe confusion is expected among most of the vegetated classes.

### C. Unmixing

The FCLSU method described in Section III-A was applied to each of the seven MERIS images and to the multitemporal time series using the 12 endmembers shown in Fig. 4. After that, fractions for the four classes case were computed by aggregating the unmixed fractions of vegetated classes into a single vegetation class and the unmixed fractions of greenhouses and built-up into a single built-up class. The fractions (12-and 4-class cases) were then compared with the reference fractions $f_c^t$ generated according to the viewing geometry of each date (monotemporal unmixing) and with the fractions $f_c^T$ generated while aggregating the LGN5 from 25 to 300 m (multitemporal unmixing). The OSA (9) was used to do this comparison.

Tables I and II summarize the results of the subpixel and per-pixel classification accuracy assessment for the 12- and 4-class cases. Results are moderately good, and as expected, the four-class case offers better OSA and overall accuracy (OA) values because the spectral confusion among vegetated classes is removed (e.g., mean OSA values for the multitemporal unmixing of 83% versus 53%). Additionally, these tables show that the OSA and OA values are in the same order of magnitude. However, the OSA was computed with subpixel fractions, and therefore, it inherently contains more information than the OA, which was computed from the hard classified images at 300 m. Furthermore, the multitemporal approach yielded classification results very similar to the ones obtained from the best monotemporal image (April). This might indicate that the selection of the dates for the unmixing is critical (e.g., in spring most of the vegetated classes appear to have a large separability). This might also indicate that gridding artifacts introduced during the reprojection of the MERIS FR images into a common grid (and ultimately introduced when the MERIS L1b products were generated by ESA) might "cancel out" the benefits of using temporal information for the unmixing of heterogeneous areas. This is because the ground fractions that "generate" the mixed signal for each MERIS multitemporal pixel element are not constant but we use constant fractions $(\omega^T)$ to validate the results.

As an example, Fig. 5 shows the OSA for the multitemporal unmixing of 12 classes and for the four-class aggregated results. This figure can be used to spatially validate the unmixing results. In general, we observe that homogeneous areas tend to agree well with the reference data set. Nonetheless, the 12-class OSA (Fig. 5, left panel) shows low agreements in the northeast and in the southeast of The Netherlands. These low-accuracy areas are rather heterogeneous and were unmixed using fewer dates (see Fig. 2).

Fig. 6 shows the hard classifications obtained from the multitemporal unmixing (12 and 4 classes) as well as the corresponding reference data sets. Notice that the gap in the inland waters of the north of The Netherlands is caused by the atmospheric correction as only the first 10 km of coastal water could be atmospherically corrected (and, therefore, we decided to mask out all pixels that were uncorrected). This negatively affects the mean OSA and the OA values as we masked out "homogenous" water pixels, which are relatively easy to unmix. In this respect, we believe that our results compare well with "classical" (per-pixel) classifications over the same area and with the same sensor. In [30], OA values on the order of 67% were found for seven common land-cover types, while we got OA values of about 55% and 88% for 12 and 4 land-cover classes while excluding most of the homogeneous areas.

Tables III and IV present the user's and producer's accuracies of the hard classifications. There, one can see that the classes orchards, swamps, and winter crops present the three poorest producer's and user's accuracies followed by the classes heathlands, bare soil, and deciduous forest (Table III). These low accuracies support the thematic aggregation of the results from 12 to 4 classes. Notice that, after the aggregation, only bare soil presents poor user's and producer's accuracies, and this is because residual clouds were classified as bare soil. This can be seen in Fig. 6 as a narrow and scattered bare soil band that crosses The Netherlands from west to east at the latitude of the northeast polder both in the 12- and 4-class hard classification results.

Finally, the multitemporal results were also analyzed with respect to homogeneity. The multitemporal SPI (Section III-B) was used to group the pixels into three homogeneity categories of approximately equal number of pixels (33% of The Netherlands each group). The three SPI categories were composed as follows: 1) SPI values smaller than 0.6 (33.5% of the total number of pixels); 2) SPI values between 0.6 and 0.9 (36.1%); and 3) SPI values greater than 0.9 (31.4%). Table V shows that the higher the SPI values (homogeneous areas), the higher the accuracy of the results. Recall that the multitemporal SPI is computed from the land-cover fractions of the LGN5 at 25 m. Thus, the areas with low SPI values are areas where the land-cover classes within the observed footprint at each MERIS acquisition date are slightly different due to the different orbits and observation geometries. This might explain the low multitemporal classification accuracy results: In areas where the multitemporal pixel composition is variable, the accuracy is poor, and in areas where the multitemporal pixel composition is homogeneous, the accuracy is moderate to good.

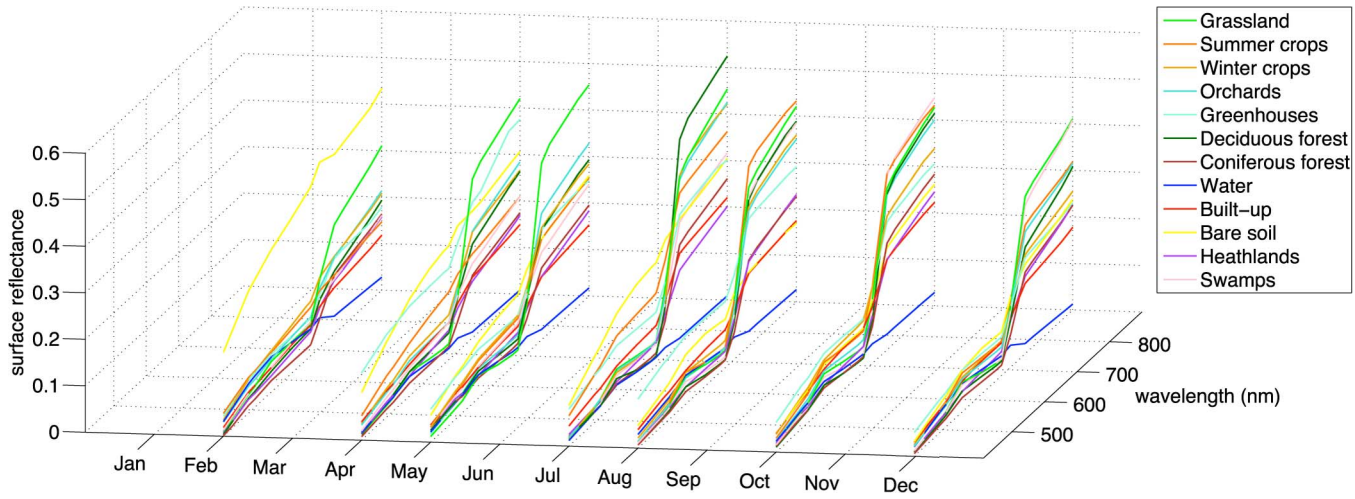


Fig. 4. Spectral signature of the endmembers extracted from the MERIS FR time series.

TABLE I
SUMMARY OF THE ACCURACY ASSESSMENT FOR THE 12-CLASS CASE

| Date | 18-2-2003 | 16-4-2003 | 31-5-2003 | 14-7-2003 | 6-8-2003 | 15-10-2003 | 8-12-2003 | Multitemp |
|---|---|---|---|---|---|---|---|---|
| mean OSA | 43.54 | 52.70 | 42.35 | 45.46 | 36.88 | 41.56 | 44.78 | 52.72 |
| Std. OSA | 30.68 | 31.01 | 31.44 | 31.31 | 31.32 | 34.55 | 34.06 | 28.77 |
| Kappa | 0.33 | 0.44 | 0.33 | 0.36 | 0.27 | 0.30 | 0.32 | 0.45 |
| OA | 44.29 | 54.17 | 43.88 | 46.06 | 35.29 | 41.87 | 45.68 | 55.17 |

OSA=overall sub-pixel accuracy; std=standard deviation; OA=overall accuracy.

TABLE II
SUMMARY OF THE ACCURACY ASSESSMENT FOR THE FOUR-CLASS CASE

| Date | 18-2-2003 | 16-4-2003 | 31-5-2003 | 14-7-2003 | 6-8-2003 | 15-10-2003 | 8-12-2003 | Multitemp |
|---|---|---|---|---|---|---|---|---|
| mean OSA | 77.20 | 82.84 | 78.21 | 83.07 | 80.01 | 74.52 | 74.28 | 82.51 |
| Std. OSA | 24.97 | 18.83 | 22.04 | 20.96 | 24.50 | 27.71 | 27.75 | 19.48 |
| Kappa | 0.52 | 0.73 | 0.60 | 0.69 | 0.58 | 0.50 | 0.50 | 0.71 |
| OA | 80.83 | 88.27 | 83.09 | 87.28 | 82.54 | 76.66 | 77.56 | 87.81 |

OSA=overall sub-pixel accuracy; std=standard deviation; OA=overall accuracy.

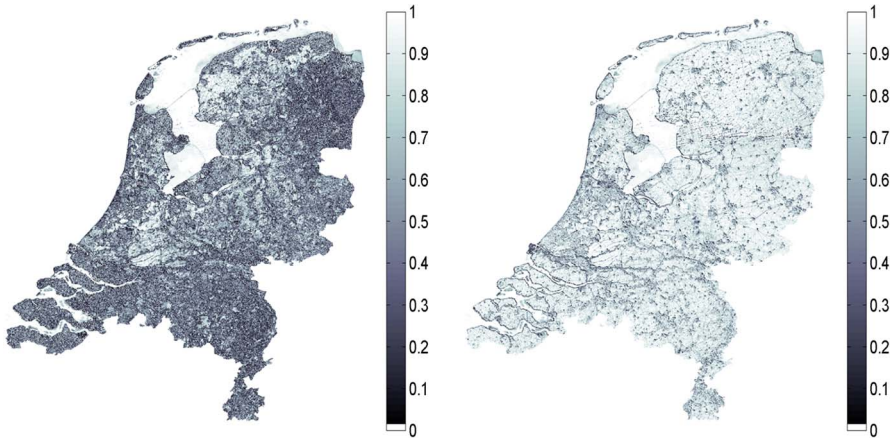


Fig. 5. Overall subpixel accuracies (OSA) for the multitemporal unmixing of (left) 12 and (right) 4 classes.

Last but not least, one should realize that, first, the validation might be affected by residual preprocessing errors (e.g., geolocation) or other sensor specific issues like the point spread function of the sensor, which might result in validation errors even if the fractions are correctly retrieved by the linear unmixing model [31], [32]. Second, the endmembers were produced by averaging "pure" pixels of each land-cover type. Accounting for endmember variability, for instance, the use of a Monte Carlo approach [17] or the use of endmember bundles [33] might result in improved results. Third, our validation analysis relies

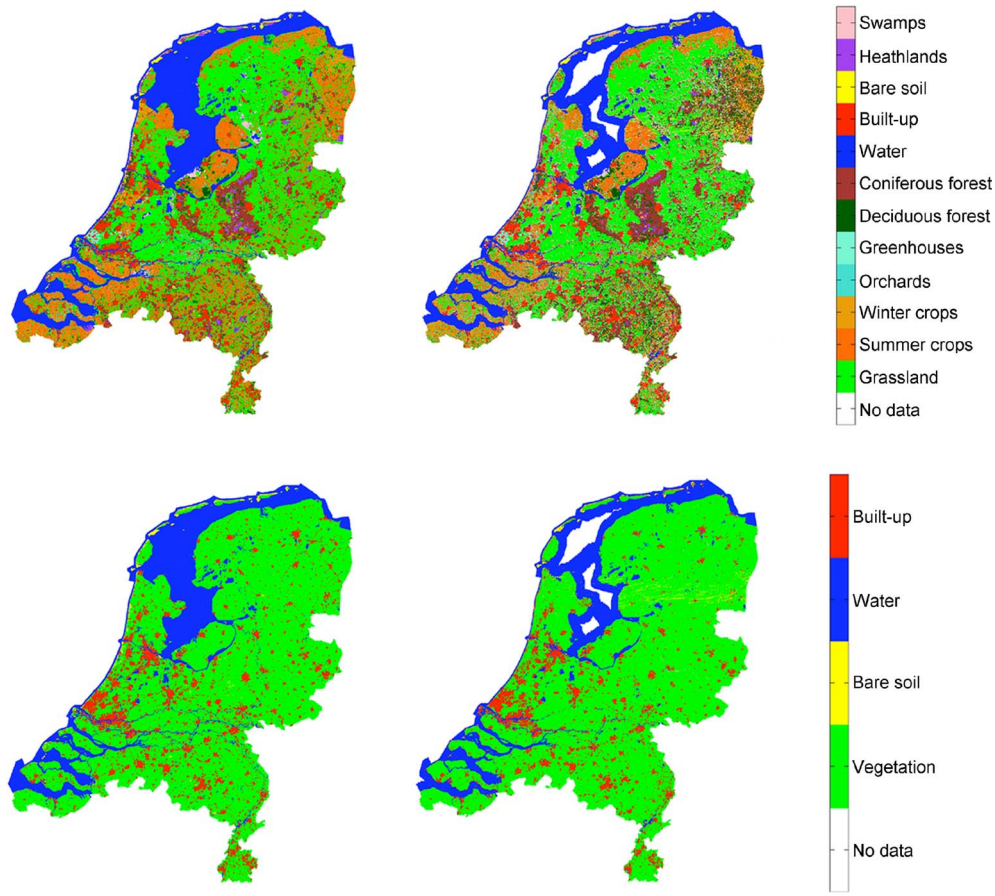


Fig. 6. (Left) Reference data set and (right) multitemporal hard classified images for (top row) 12 and (bottom row) 4 classes.

TABLE III
USER'S AND PRODUCER'S ACCURACIES (UA AND PA, RESPECTIVELY) FOR THE MULTITEMPORAL UNMIXING OF THE 12-CLASS CASE

| Class | Grassland | Summer Crops | Winter Crops | Orchards | Greenhouses | Deciduous. Forest |
|---|---|---|---|---|---|---|
| UA | 70.96 | 58.40 | 17.59 | 4.19 | 16.27 | 13.40 |
| PA | 72.90 | 26.29 | 18.58 | 0.97 | 68.66 | 35.79 |
| Class | Coniferous Forest | Water | Built-up | Bare soil | Heathlands | Swamps |
| UA | 50.09 | 86.95 | 71.67 | 10.79 | 13.72 | 5.05 |
| PA | 71.78 | 88.70 | 41.45 | 37.17 | 31.88 | 15.17 |

TABLE IV
USER'S AND PRODUCER'S ACCURACIES (UA AND PA, RESPECTIVELY) FOR THE MULTITEMPORAL UNMIXING OF THE 4-CLASS CASE

| Class | Vegetation | Bare soil | Water | Built-up |
|---|---|---|---|---|
| UA | 87.58 | 36.65 | 92.55 | 78.42 |
| PA | 98.05 | 24.71 | 84.79 | 25.59 |

TABLE V
COHEN'S KAPPA AND OA FOR THE MULTITEMPORAL CASE GROUPED BASED ON SPI CLASSES

| Classes | Statistical | SPI<0.6 | 0.6<SPI<0.9 | SPI>0.9 |
|---|---|---|---|---|
| 12 | Kappa | 0.16 | 0.41 | 0.79 |
| | OA | 29.29 | 53.84 | 85.34 |
| 4 | Kappa | 0.27 | 0.56 | 0.90 |
| | OA | 81.88 | 87.73 | 94.46 |

on a static data set based on high-spatial-resolution images from 2003 and 2004 and that is also subjected to classification errors [34]. Nonetheless, this database was considered appropriate for our validation analysis given the basic thematic aggregation level considered in this study (12 classes) and the temporal stability of these classes in The Netherlands [34].

## V. CONCLUSION

In this paper, a time series of MERIS FR acquisitions was used to spectrally unmix the 12 most important land-cover classes in The Netherlands. The unmixing was done both for each image (monotemporal) and by layer stacking all the images in the time series (multitemporal). The aim of this unmixing exercise was to evaluate the capabilities of MERIS FR time series to deliver information comparable with the one that can be obtained from high-spatial-resolution (Landsat-like) land-cover data sets. In this case, the Dutch national land-cover map (LGN5; 12 classes) was used to validate the unmixing

results both at subpixel (OSA) and at per-pixel (OA and Kappa) levels.

Validation results showed that the multitemporal unmixing yielded subpixel (mean OSA) and per-pixel (OA) accuracies very similar to the ones obtained for the best monotemporal image (the image of April). More precisely, the OA results were moderate (around 55%). This indicates the following: 1) The selection of dates used for the unmixing is critical; 2) the spectral confusions occurred during the unmixing, and thus, vegetation phenophases and the spectral class separability must be further studied in order to optimize the best combination of dates and classes to be unmixed; and 3) MERIS gridding artifacts in combination with the spatial heterogeneity of the landscape might "cancel out" the synergies of using spectral and temporal information for the unmixing of heterogeneous areas.

In order to reduce spectral confusion, the unmixing results were aggregated to the four main classes. This aggregation step considerably increased the classification accuracy (OA values about 88%), and again, the multitemporal case yielded very similar results to the ones obtained with the image acquired in April.

Additionally, one should keep in mind the following aspects. First, this work uses a time series of seven MERIS images because of the extensive and frequent cloud coverage in The Netherlands. In this respect, clouds might be a limiting factor for multitemporal studies as they might mask important vegetation phenophases. Second, residual preprocessing uncertainties (like geolocation or cloud masking) and the use of only one endmember per land-cover type might have a negative effect on the validation results. Third, the validation is based on a static data set produced using a combination of high-resolution satellite data from 2003 and 2004 and several sources of ancillary data. This means that the validation might be affected by the production period and by its classification accuracy. Fourth, these results refer to truly heterogeneous areas since the majority of the pixels over "homogeneous" inland waters were excluded from the analysis.

Finally, it is remarkable that, for both aggregation levels (12 and 4 classes), the mean OSA values are very similar to the OA values, whereas the former is computed using subpixel fractions; thus, it essentially contains more information than the latter. Therefore, we are confident that the extracted subpixel information might be of great utility in remote sensing monitoring activities, such as land-cover change detection or retrieval of biophysical parameters from medium-spatial-resolution data acquired over heterogeneous and frequently clouded areas.

## REFERENCES


[1] P. M. Atkinson, "The importance of scale in remote sensing and GIS and its implications for data integration," in *Integration of GIS and Remote Sensing*, V. Mesev, Ed. Chichester, U.K.: Wiley, 2007, p. 296.

[2] P. A. Burrough and R. A. McDonnell, *Principles of Geographical Information Systems*. Oxford, U.K.: Oxford Univ. Press, 1998.

[3] P. Fisher, "The pixel: A snare and a delusion," *Int. J. Remote Sens.*, vol. 18, no. 3, pp. 679–685, Feb. 1997.

[4] R. P. Napelka and P. D. Hyde, "Classifying unresolved objects from simulated space data," in *Proc. 8th Int. Symp. Remote Sens. Environ.*, Ann Arbor, MI, 1972, pp. 935–949.

[5] R. S. Chikara, "Effect of mixed (boundary) pixels on crop proportion estimation," *Remote Sens. Environ.*, vol. 14, no. 1–3, pp. 207–218, Jan. 1984.

[6] F. J. Gallego, "Remote sensing and land cover area estimation," *Int. J. Remote Sens.*, vol. 25, no. 15, pp. 3019–3047, Aug. 2004.

[7] S. Garrigues, D. Allard, F. Baret, and M. Weiss, "Influence of landscape spatial heterogeneity on the non-linear estimation of leaf area index from moderate spatial resolution remote sensing data," *Remote Sens. Environ.*, vol. 105, no. 4, pp. 286–298, Dec. 2006.

[8] B. Tan, J. Hu, P. Zhang, D. Huang, N. Shabanov, M. Weiss, Y. Knyazikhin, and R. B. Myneni, "Validation of moderate resolution imaging spectroradiometer leaf area index product in croplands of Alpilles, France," *J. Geophys. Res. D: Atmospheres*, vol. 110, pp. 1–15, 2005.

[9] Y. Tian, R. E. Dickinson, L. Zhou, X. Zeng, Y. Dai, R. B. Myneni, Y. Knyazikhin, X. Zhang, M. Friedl, H. Yu, W. Wu, and M. Shaikh, "Comparison of seasonal and spatial variations of leaf area index and fraction of absorbed photosynthetically active radiation from Moderate Resolution Imaging Spectroradiometer (MODIS) and common land model," *J. Geophys. Res. D: Atmospheres*, vol. 109, p. D01 103, 2004.

[10] A. Simic, J. M. Chen, J. Liu, and F. Csillag, "Spatial scaling of net primary productivity using subpixel information," *Remote Sens. Environ.*, vol. 93, no. 1/2, pp. 246–258, Oct. 2004.

[11] Y. J. Kaufman, L. Remer, and D. Tanré, "A critical examination of the residual cloud contamination and diurnal sampling effects on MODIS estimates of aerosol over ocean," *IEEE Trans. Geosci. Remote Sens.*, vol. 43, no. 12, pp. 2886–2897, Dec. 2005.

[12] M. Rast, J. L. Bezy, and S. Bruzzi, "The ESA medium resolution imaging spectrometer MERIS—A review of the instrument and its mission," *Int. J. Remote Sens.*, vol. 20, no. 9, pp. 1681–1702, 1999.

[13] N. Keshava, "A survey of spectral unmixing algorithms," *Lincoln Lab. J.*, vol. 14, no. 1, pp. 55–78, Jan. 2003.

[14] N. Keshava and J. F. Mustard, "Spectral unmixing," *IEEE Signal Process. Mag.*, vol. 19, no. 1, pp. 44–57, Jan. 2002.

[15] F. Poulet and S. Erard, "Nonlinear spectral mixing: Quantitative analysis of laboratory mineral mixtures," *J. Geophys. Res. E: Planets*, vol. 109, pp. E02 009-1–E02 009-12, 2004.

[16] B. Somers, K. Cools, S. Delalieux, J. Stuckens, D. Van der Zande, W. W. Verstraeten, and P. Coppin, "Nonlinear hyperspectral mixture analysis for tree cover estimates in orchards," *Remote Sens. Environ.*, vol. 113, no. 6, pp. 1183–1193, Jun. 2009.

[17] D. B. Lobell and G. P. Asner, "Cropland distribution from temporal unmixing of MODIS data," *Remote Sens. Environ.*, vol. 93, no. 3, pp. 412–422, Nov. 2004.

[18] M. Ozdogan, "The spatial distribution of crop types from MODIS data: Temporal unmixing using independent component analysis," *Remote Sens. Environ.*, vol. 114, no. 6, pp. 1190–1204, Jun. 2010.

[19] L. Gomez-Chova, G. Camps-Valls, J. Calpe-Maravilla, L. Guanter, and J. Moreno, "Cloud-screening algorithm for ENVISAT/MERIS multispectral images," *IEEE Trans. Geosci. Remote Sens.*, vol. 45, no. 12, pp. 4105–4118, Dec. 2007.

[20] L. Guanter, L. Gómez-Chova, and J. Moreno, "Coupled retrieval of aerosol optical thickness, columnar water vapor and surface reflectance maps from ENVISAT/MERIS data over land," *Remote Sens. Environ.*, vol. 112, no. 6, pp. 2898–2913, Jun. 2008.

[21] L. Guanter, A. Ruiz-Verdú, O. Odermatt, C. Giardino, S. Simis, V. Estellés, T. Heege, J. A. Domínguez-Gómez, and J. Moreno, "Atmospheric correction of ENVISAT/MERIS data over inland waters: Validation for European lakes," *Remote Sens. Environ.*, vol. 114, no. 3, pp. 467–480, Mar. 2010.

[22] G. Hazeu, The Dutch Land Use Database LGN [Accessed Jun. 16, 2010]. 2005. [Online]. Available: http://www.lgn.nl/

[23] J. J. Settle and N. A. Drake, "Linear mixing and the estimation of ground cover proportions," *Int. J. Remote Sens.*, vol. 14, no. 6, pp. 1159–1177, Apr. 1993.

[24] C. Ichoku and A. Karnieli, "A review of mixture modeling techniques for sub-pixel land cover estimation," *Remote Sens. Rev.*, vol. 13, no. 3/4, pp. 161–186, Apr. 1996.

[25] D. C. Heinz and C. I. Chang, "Fully constrained least squares linear spectral mixture analysis method for material quantification in hyperspectral imagery," *IEEE Trans. Geosci. Remote Sens.*, vol. 39, no. 3, pp. 529–545, Mar. 2001.

[26] L. Gómez-Chova, R. Zurita-Milla, L. Alonso, J. Amorós-López, L. Guanter, and G. Camps-Valls, "Gridding artifacts on medium-resolution satellite image time series: MERIS case study," *IEEE Trans. Geosci. Remote Sens.*, 2011, accepted for publication.

[27] A. Plaza, P. Martínez, R. Pérez, and J. Plaza, "A quantitative and comparative analysis of endmember extraction algorithms from hyperspectral

data," *IEEE Trans. Geosci. Remote Sens.*, vol. 42, no. 3, pp. 650–663, Mar. 2004.
[28] R. Zurita-Milla, J. G. P. W. Clevers, M. E. Schaepman, and M. Kneubuehler, "Effects of MERIS L1b radiometric calibration on regional land cover mapping and land products," *Int. J. Remote Sens.*, vol. 28, no. 3/4, pp. 653–673, Feb. 2007.
[29] M. A. Theseira, G. Thomas, J. C. Taylor, F. Gemmell, and J. Varjo, "Sensitivity of mixture modelling to end-member selection," *Int. J. Remote Sens.*, vol. 24, no. 7, pp. 1559–1575, Apr. 10, 2003.
[30] J. G. P. W. Clevers, M. E. Schaepman, C. A. Mücher, A. J. W. de Wit, R. Zurita-Milla, and H. M. Bartholomeus, "Using MERIS on Envisat for land cover mapping in the Netherlands," *Int. J. Remote Sens.*, vol. 28, no. 3/4, pp. 637–652, Feb. 2007.
[31] J. J. Settle, "On the residual term in the linear mixture model and its dependence on the point spread function," *IEEE Trans. Geosci. Remote Sens.*, vol. 43, no. 2, pp. 398–401, Feb. 2005.
[32] J. R. G. Townshend, C. Huang, S. N. V. Kalluri, R. S. Defries, S. Liang, and K. Yang, "Beware of per-pixel characterization of land cover," *Int. J. Remote Sens.*, vol. 21, no. 4, pp. 839–843, 2000.
[33] C. A. Bateson, G. P. Asner, and C. A. Wessman, "Endmember bundles: A new approach to incorporating endmember variability into spectral mixture analysis," *IEEE Trans. Geosci. Remote Sens.*, vol. 38, no. 2, pp. 1083–1094, Mar. 2000.
[34] G. W. Hazeu, "Land use mapping and monitoring in The Netherlands (LGN5)," in *Proc. 2nd Workshop EaRSeL SIG Remote Sens. Land Use Land Cover*, Bonn, Germany, 2006, pp. 323–329.

**Raúl Zurita-Milla** received the B.S. degree in agricultural engineering from the University of Córdoba, Córdoba, Spain, in 2003 and the M.Sc. degree (with distinction) in geoinformation science and the Ph.D. degree in remote sensing from Wageningen University, Wageningen, The Netherlands, in 2003 and 2008, respectively.

Since 2008, he has been an Assistant Professor with the Department of Geo-Information Processing, Faculty of Geo-Information Science and Earth Observation (ITC), University of Twente, Enschede, The Netherlands. His current research interests are on multiscale data integration.

**Luis Gómez-Chova** (S'08–M'09) received the B.Sc. (with first-class honors), M.Sc., and Ph.D. degrees in electronics engineering from the University of Valencia, Valencia, Spain, in 2000, 2002 and 2008, respectively.

Since 2000, he has been with the Department of Electronics Engineering, University of Valencia, where he is currently an Assistant Professor. He is also a Researcher with the Image Processing Laboratory, University of Valencia, where his work is mainly related to pattern recognition and machine learning applied to remote sensing multispectral images and cloud screening.

**Luis Guanter** received the B.Sc. degree (with first-class honors) in physics and the M.Sc. and Ph.D. degrees in environmental physics and thermodynamics from the University of Valencia, Valencia, Spain, in 2002, 2004, and 2007, respectively.

Since February 2011, he has been a Marie Curie Postdoctoral Fellow with the Atmospheric, Oceanic and Planetary Physics, Clarendon Laboratory, University of Oxford, Oxford, U.K. His research interests in remote sensing include data preprocessing, the retrieval of atmospheric components, and the definition of future satellite missions. He is a member of the ESA Sentinel-2 Mission Advisory Group and the PROBA-V International Users Committee.

**Jan G. P. W. Clevers** holds the M.Sc. degree in agronomy and the Ph.D. degree in remote sensing from Wageningen University, Wageningen, The Netherlands, in 1981 and 1986.

Currently, he is an Associate Professor and Lecturer in remote sensing with Wageningen University. His current research activities concern the developments of optical reflectance models (including bidirectional reflectance and hyperspectral measurements), the linking to crop growth models, the synergy hypothesis with the purpose of the combined use of optical and microwave observations as well as of prior knowledge, and land-cover mapping using remote sensing data at different scales.

**Gustavo Camps-Valls** (M'04–SM'07) received the B.Sc. degree in physics, the M.Sc. degree in electronics engineering, and the Ph.D. degree in physics from the University of Valencia, Valencia, Spain, in 1996, 1998, and 2002, respectively.

He is currently an Associate Professor with the Department of Electronics Engineering and a Member of the Image Processing Laboratory, University of Valencia. He is interested in the development of machine learning algorithms for signal and image processing. He is a referee of many international journals and conferences.